

---

# Parametric Images of Myocardial Metabolic Rate of Glucose Generated from Dynamic Cardiac PET and 2-[<sup>18</sup>F]Fluoro-2-deoxy-d-glucose Studies

Yong Choi, Randall A. Hawkins, Sung-Cheng Huang, Sanjiv S. Gambhir, Richard C. Brunken, Michael E. Phelps, and Heinrich R. Schelbert

*Division of Nuclear Medicine and Biophysics, Department of Radiological Sciences, Laboratory of Nuclear Medicine (DoE), and The Crump Institute, UCLA School of Medicine, Los Angeles, California*

---

We describe a method for generating parametric images of the myocardial metabolic rate of glucose (MMRGlc) with positron emission tomography (PET). The method employs serially acquired images of 2-[<sup>18</sup>F]fluoro-2-deoxy-D-glucose (FDG) uptake and a Patlak graphical analysis of the image data. The arterial input function is derived from images of the left ventricular blood pool calibrated with <sup>18</sup>F-plasma measurements. The approach is computationally fast enough to be used in a clinical environment. The MMRGlc parametric images improve myocardial contrast relative to non-parametric images, especially in studies with poor myocardial uptake of FDG. In addition, MMRGlc parametric images consolidate the large amount of data in a dynamic PET study into a clinically usable image set.

**J Nucl Med 1991; 32:733-738**

---

The myocardial metabolic rate of glucose (MMRGlc) can be measured with positron emission tomography (PET) and 2-[<sup>18</sup>F]fluoro-2-deoxy-D-glucose (FDG) using an appropriate modification of the technique originally developed by Sokoloff et al. (1) for the measurement of cerebral glucose utilization (2-6). The three-compartment model used in this technique has been validated in rabbit and canine myocardium under different physiologic states (7-9).

While the quantification of MMRGlc requires dynamic PET-FDG studies, visual interpretation of FDG studies is usually based on one static image obtained about 40 min after injection. In this work, we describe a method to produce parametric (pixel-by-pixel) images of MMRGlc to incorporate quantitative information from dynamic

studies into the clinical visual interpretation process (10). MMRGlc parametric images reflect the glucose metabolic rate directly, rather than count density. Parametric images not only facilitate quantification of regional MMRGlc (images are scaled directly in units of glucose metabolism) but also improve the quality of the images and the information content of the image by suppressing noise and amplifying the useful information (signal) of the image. Additionally, parametric images are ideally suited to a clinical environment in which efficient data processing and image presentation are primary requirements. One application of parametric images of MMRGlc is therefore in the now evolving arena of clinical PET.

Gambhir et al. (11) developed a computationally simplified method for estimating regional MMRGlc with FDG using a Patlak graphical analysis method that employs an input function derived from a time-activity curve from the left ventricular blood pool. This method reduces the number of plasma samples that are required to quantify MMRGlc from a completely determined arterial input function (about 30 samples for a 1-hr study) to a number necessary to calibrate the noninvasively derived arterial input function (three samples). This graphical method is well suited for parametric imaging because nonlinear regression is not required and the method is computationally efficient.

## MATERIALS AND METHODS

### Human Subjects

One normal volunteer, one diabetic, and eight non-diabetic patients with a history of coronary artery disease were studied. These subjects, ages 28 to 79, were chosen to reflect a range of flow and metabolic rates to test the parametric imaging algorithm in both normal and abnormal myocardium. One of the non-diabetic patients and the one diabetic patient were studied after an overnight fast. The normal volunteer and eight of the patients were studied after receiving 50 g of glucose orally (Trutol) 1 hr prior to the FDG injection to enhance uptake of FDG by the myocardium. One patient was studied twice, once while fasting,

---

Received Jan. 6, 1990; revision accepted Oct. 30, 1990.  
For reprints contact Randall A. Hawkins, MD, PhD, Division of Nuclear Medicine and Biophysics, Department of Radiological Sciences, UCLA School of Medicine, Los Angeles, CA.

and again after glucose administration to examine the effects of substrate availability on MMRGlc.

### Image Acquisition and Analysis

After recording a 20 min blank scan and a 20 min transmission scan for photon attenuation correction, both  $^{13}\text{NH}_3$  and FDG studies were performed on a Siemens/CTI 931/08-12 tomograph. This device produces 15 simultaneous image planes encompassing a 108.0-mm axial field of view. For the patient who had both a fasting and a postprandial study, only FDG studies were performed.

The  $^{13}\text{NH}_3$  protocol included an intravenous injection of 20 mCi  $^{13}\text{NH}_3$  and dynamic image acquisition consisting of twelve 10-sec, two 60-sec, and three 300-sec frames. After a 50-min delay for  $^{13}\text{N}$  decay, 10 mCi FDG were injected intravenously and serial images obtained for 54 min in a sequence of twelve 10-sec, four 30-sec, two 300-sec, and four 600-sec frames.

Cross-sectional images were reconstructed employing a Shepp-Logan filter with a cut-off frequency of  $0.15 \text{ mm}^{-1}$ , yielding a spatial resolution of  $\sim 10 \text{ mm}$  FWHM in plane. In some studies, interplane summing among adjacent three planes with a weighting factor 1:2:1 was performed to reduce noise.

The  $^{13}\text{NH}_3$  studies were acquired to delineate myocardial blood flow and to identify blood flow/metabolism imbalances as a part of other investigative protocols. The  $^{13}\text{NH}_3$  studies also permitted a preliminary comparison of myocardial perfusion to the parametric images of myocardial glucose metabolism generated in this project. Two observers compared MMRGlc parametric images to  $^{13}\text{NH}_3$  flow images to identify myocardial regions that were normal, regions that were hypoperfused and exhibited preserved glucose metabolism and regions that were hypoperfused with reduced glucose metabolism.

### Blood Samples and Calibration

The subject's hand was heated (12-13) and three 5-cc venous blood samples were obtained at 24, 34, and 44 min after FDG injection. Fluorine-18-plasma activity concentration was measured in a well counter following centrifugation of each sample. The blood activity was used to correct for spillover of activity from myocardial tissue to left ventricular blood pool and to determine the plasma glucose concentration at the time of the scan.

A cylinder phantom containing  $^{68}\text{Ge}/^{68}\text{Ga}$  was scanned after each study to evaluate the plane efficiency of the tomograph and to determine the conversion factor between image data in units of counts/pixel/sec and well counter data in units of counts/ml/sec.

### Calculation of MMRGlc

The three-compartment model for FDG consists of FDG in plasma ( $C_p^*$ ), FDG in tissue ( $C_t^*$ ), and FDG-6-phosphate in tissue ( $C_m^*$ ) (4,13). The first-order rate constants,  $k_1^*$  and  $k_2^*$  refer to forward and reverse transport of FDG across the capillary and sarcolemmal membranes while  $k_3^*$  and  $k_4^*$  refer to phosphorylation of FDG and dephosphorylation of FDG-6-phosphate, respectively. MMRGlc can be estimated from the expression

$$\text{MMRGlc} = K(C_p/\text{LC}), \quad \text{Eq. 1}$$

where  $C_p$  is the plasma glucose concentration and LC is the lumped constant that accounts for differences in the transport and phosphorylation between FDG and glucose (1,4,13). K is a

macroparameter equal to  $k_1^*k_3^*/(k_2^* + k_3^*)$ . A value of 0.67 was used for LC in this study (9).

The macroparameter K can be obtained either by fitting the FDG model to the measured tissue time-activity curves or by employing Patlak graphical analysis (11). In the former approach, after solving the differential equations governing the FDG model, least-squares nonlinear regression was performed to obtain the microparameters,  $k_1^*$  to  $k_4^*$  and a fifth parameter,  $\text{SP}_{\text{CT}}$ , to account for the chamber to tissue spillover fraction and the vascular component in the measured myocardial tissue activity (3,11).

The Patlak method employed to determine the macroparameter, K, based upon the following equation (14,15):

$$C_i^*(t)/C_p^*(t) = K \left[ \int_0^t C_p^*(\tau) d\tau \right] / C_p^*(t) + V, \quad \text{Eq. 2}$$

where  $C_i^*(t)$ , which is equal to the sum of  $C_c^*$  and  $C_m^*$  for the three compartment FDG model, is the measured myocardial tissue activity concentration at time t;  $C_p^*(t)$  is the arterial input function at time t; and V is related to the effective distribution volume of the tracer  $^{18}\text{F}$ FDG. K was estimated from the slope of the graph,  $C_i^*(t)/C_p^*(t)$  (vertical (Y) axis) versus  $[\int_0^t C_p^*(\tau) d\tau / C_p^*(t)]$  (horizontal (X) axis), with the assumption of  $k_4^*$  equal to zero. An equation,  $(n\sum XY - \sum X\sum Y)/(n\sum X^2 - (\sum X)^2)$ , for estimating the slope based on linear regression was employed to obtain K values for each pixel.

The effect of the number of time points on estimating the slope K of the Patlak plot and the parametric images of MMRGlc was examined. Computational time decreases as the number of  $C_i^*(t)$  points (number of image frames) included in the analysis is decreased. It is necessary to define the impact of the number of images used on the numerical accuracy of K estimates in order to develop a protocol optimized for both efficiency and accuracy. Twenty-two, 11 (every other frame), 6 (last 6 frames), and 3 (frames at 6.5, 29, and 39 min after injection) of the 22 dynamically acquired image frames were used in the analysis and its effect on the estimated MMRGlc on the parametric images examined. The employed image frames were weighted in proportion to scan duration time.

The input function was obtained from the left ventricular blood-pool time-activity curve, LV(t). LV(t) was generated from a small region of interest (ROI), with an area of about  $0.8 \text{ cm}^2$ , assigned to the left ventricular cavity on the dynamic PET images. It was obtained from a single plane which contained the largest left ventricular chamber and used as the arterial input function. This input function required correction for spillover of activity between left ventricular blood pool and myocardium. Additionally, because the Patlak method is based upon an assumed unidirectional net uptake of  $^{18}\text{F}$  over the duration of measurement (i.e.  $k_4^*$  assumed to be negligibly small), correcting for non-zero values of  $k_4^*$  is required, as previously described by Gambhir et al. (11).

In order to estimate  $k_4^*$  and  $\text{SP}_{\text{CT}}$  for the entire left ventricular myocardium, the last three points of LV(t), which are more affected by spillover of activity from myocardium to the blood pool than earlier points, were replaced by the in vitro measured blood activity concentrations determined at the time of these images. The rate constants  $k_1^*$  to  $k_4^*$  and  $\text{SP}_{\text{CT}}$  were obtained by fitting the FDG model to the global myocardial kinetic data,  $C_{ig}^*(t)$ , using this modified LV(t) curve. Then, the spillover corrected left ventricular blood-pool time-activity curve input func-

tion,  $C_p^*(t)$ , was generated by the following expression:

$$C_p^*(t) = LV(t) - SP_{TC} \times [SP_{CT} \text{ Corrected } C_{ig}^*(t)]. \quad \text{Eq. 3}$$

$SP_{TC}$ , the three-dimensional spillover of activity fraction from the myocardial tissue to left ventricular blood pool, is defined by:

$$SP_{TC} = (1/3) \sum_{i=1}^3 [LV(t_i) - \text{blood}(t_i)] / [SP_{CT} \text{ corrected } C_{ig}^*(t_i)], \quad \text{Eq. 4}$$

where  $\text{blood}(t_i)$  is the three plasma  $^{18}\text{F}$  concentration data at time  $t_i$ .  $[SP_{CT} \text{ Corrected } C_{ig}^*(t)]$  in Equations 3 and 4 equals  $C_{ig}^*(t) - SP_{CT} \times LV(t)$  and represents the global myocardium kinetic curve that has been corrected for spillover from blood pool to myocardial tissue and vascular component.

The  $k_4^*$  effects were taken into account after the response of the FDG model was calculated for various values of the  $k_4^*$ , while the values for  $k_1^*$  to  $k_3^*$  and  $SP_{CT}$  were fixed. The correction factor to compensate for the underestimation of tissue activity was determined by taking the ratio of the calculated tissue activity obtained with a  $k_4^*$  value from a global myocardial ROI versus that obtained with  $k_4^*$  set to zero. This factor was applied to all pixels of the images that were employed for calculating the slope  $K$  with Equation 2. A simulation was performed to examine the magnitude of non-zero  $k_4^*$  correction as a function of  $k_4^*$ .

### Generation of Parametric Images

The sequence of steps required to generate the parametric images was as follows:

1. Dynamic PET images were acquired for 54 min after FDG injection. Three blood samples were obtained at approximately 24, 34, and 44 min after FDG injection for measurement of plasma  $^{18}\text{F}$  concentrations.
2. A 20-cm diameter cylinder phantom filled with  $^{68}\text{Ge}/^{68}\text{Ga}$  solution was scanned and a 5-ml aliquot of the  $^{68}\text{Ge}/^{68}\text{Ga}$  solution was counted in a well counter in order to derive the conversion factor between image data and blood sample data.
3.  $k_4^*$  and  $SP_{CT}$  values were obtained by fitting the model to a global myocardial ROI using  $LV(t)$  input function with the last three points replaced by blood samples.
4. The spillover corrected left ventricular blood pool time-activity curve,  $C_p^*(t)$ , as the arterial input function was generated according to Equation 3.
5. Pixel counts at different time points (more than three) were used to estimate  $K$  for each pixel of the  $128 \times 128$  image matrix using Equation 2 with  $k_4^*$  correction.
6. A parametric image of MMRGlc was generated with values of  $C_p$ , the lumped constant, and pixel by pixel values of  $K$ .

The values of MMRGlc obtained directly from parametric images were compared to the values obtained by applying nonlinear regression and regional Patlak analysis to the tissue time-activity curves generated from selected ROI's over the same tissue region in dynamic FDG images.

### RESULTS

Figure 1 demonstrates the myocardial tissue curve, an uncorrected and spillover corrected  $LV(t)$ , and three plasma  $^{18}\text{F}$  concentrations. The corrected left ventricular

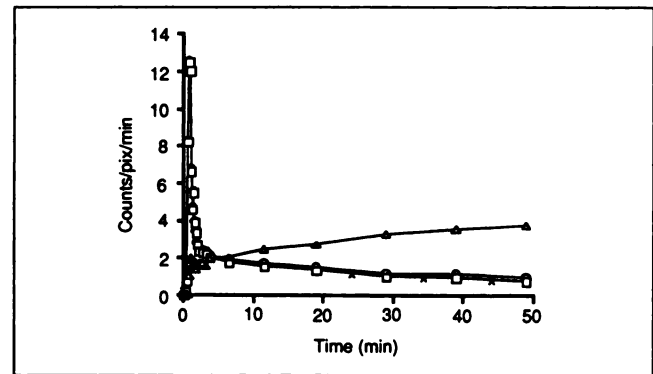


**FIGURE 1.** Kinetic data generated from an ROI over the entire left ventricular myocardium (triangles),  $C_{ig}^*(t)$ , and from the left ventricular blood pool (circles),  $LV(t)$ . Corrected blood-pool concentrations (squares),  $C_p^*(t)$ , generated using Expression 3 are lower than  $LV(t)$  because of the spillover correction. Three points marked by "x" represent in vitro blood sample data.

blood-pool time-activity curve,  $C_p^*(t)$ , which was generated using Equation 3, is usually lower than the uncorrected  $LV(t)$  directly derived from the images because the effect of spillover from tissue to blood-pool activity ( $SP_{TC}$ ) was eliminated.

The effects of the number of time points used for the Patlak plot on the parametric images are illustrated in Table 1. The total number of scans used in the analysis varied from 22 to 3. Values for MMRGlc were reproducible and stable with as few as three scan time points. The values obtained with non-linear regression are also shown.

Figure 2 illustrates a simulation of the effect of different  $k_4^*$  values on the tissue curve and Patlak derived  $K$  values while the other microparameters remain constant. Three different sets of microparameters represent high to low  $K$  values. Percent differences were obtained after calculating tissue curves for various  $k_4^*$  values and comparing Patlak slopes for tissue curves generated with zero versus non-zero values of  $k_4^*$ . The correction factor as a function of  $k_4^*$  was applied to the time points used to estimate  $K$  values after obtaining  $k_4^*$  for the entire left ventricular myocardium. If the  $k_4^*$  values were not positive, the cor-

**TABLE 1**  
The Effects of the Number of Time Points on MMRGlc Values

Number of time points	Patient 1	Patient 2
22	0.646 ± 0.084*	0.371 ± 0.029*
11	0.660 ± 0.059	0.425 ± 0.034
6	0.636 ± 0.070	0.393 ± 0.030
3	0.644 ± 0.071	0.423 ± 0.022
Nonlinear regression	0.636 ± 0.089†	0.389 ± 0.038†

\* Mean value ± standard deviation of pixel values in a global left ventricular myocardium ROI in units of  $\mu\text{mole}/\text{min}/\text{g}$ .

† Estimated value ± standard error of the estimate in units of  $\mu\text{mole}/\text{min}/\text{g}$ .

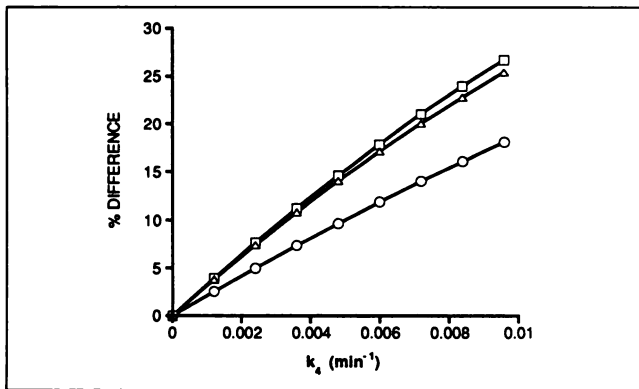


**FIGURE 2.** The effects of  $k_4^*$  values, from 0 to  $0.01 \text{ min}^{-1}$ , on the slope of the Patlak plot,  $K$ , with constant  $k_1^*$ ,  $k_2^*$ ,  $k_3^*$  and  $SP_{CT}$  values. Values for  $k_1^*$  (ml/min/g),  $k_2^*$  ( $\text{min}^{-1}$ ),  $k_3^*$  ( $\text{min}^{-1}$ ) and  $SP_{CT}$ , are, respectively, (0.59, 1.40, 0.14, 0.24) for circles, (0.55, 1.39, 0.08, 0.22) for squares, and (0.42, 1.08, 0.05, 0.20) for triangles.

rection was not performed. Among 53 serially acquired image planes in the 10 patients, five planes in 3 patients had non-zero  $k_4^*$ . The maximum value for  $k_4^*$  of  $0.0045 \text{ min}^{-1}$  caused a 9% underestimation of MMRGlc.

A typical Patlak plot to a data set from a single pixel in a normal myocardial region is illustrated in Figure 3. The computation time for generating a parametric image for a  $128 \times 128$  image was about 5 sec with a VAX 780 computer and less than a tenth of a second with a Connection Machine (16).

An unprocessed FDG image (in counts/pixel/min) obtained 49 min after injection and a parametric image of MMRGlc (in  $\mu\text{mole}/\text{min}/\text{g}$ ) are illustrated in Figure 4. Note the increased contrast, especially between blood pool and myocardium, in the parametric image. The ratio of imaged density, activity in myocardium divided by activity in left ventricular blood pool, increased from 10 to 240. The improvement in contrast is more evident when myocardial FDG uptake is low. This may occur when plasma glucose and insulin levels are low, or, as in the case of

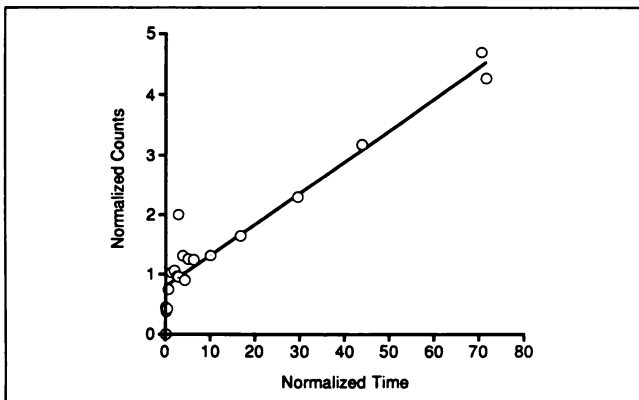


**FIGURE 3.** A linear fit of normalized time ( $[\int_0^t C_p^*(\tau) d\tau] / C_p^*(t)$ ) vs. normalized counts ( $C_i^*(t) / C_p^*(t)$ ) using a typical single pixel kinetic data set.

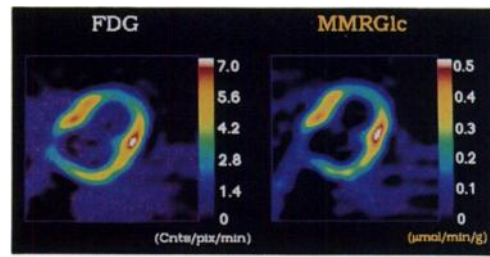


**FIGURE 4.** (Left) Unprocessed FDG image in counts/pixel/min at 49 min after injection. (Right) Parametric image which is scaled in  $\mu\text{mole}/\text{min}/\text{g}$  illustrating MMRGlc. The parametric image has higher contrast than the FDG uptake image.

diabetics, when plasma glucose level is high. These conditions can produce FDG images in which the myocardium is poorly visualized. This effect is illustrated in Figure 5, showing an FDG image at 49 min after injection and the corresponding MMRGlc parametric image. The myocardium is poorly visualized on the FDG image and, in contrast, is well defined on the MMRGlc parametric image.

Values of MMRGlc obtained from parametric images (using six time points) and the corresponding values of MMRGlc obtained from nonlinear regression and regional Patlak analysis (using 6 time points) for same region are illustrated in Table 2. The difference between parametric and regional analysis methods (nonlinear and Patlak) was not statistically and physiologically significant between groups. This indicates that the parametric imaging approach can be as accurate as regional kinetic estimates of MMRGlc.

Unprocessed FDG uptake images recorded 49 min after tracer injection and the corresponding parametric images of MMRGlc in a patient in the fasted state and after oral glucose are shown in Figure 6. Plasma glucose concentrations,  $C_p$ , increased from 85.0 to 160.9 mg/dl and insulin levels from 8 to 128  $\mu\text{U}/\text{ml}$ , respectively, from the fasting to the post glucose state. MMRGlc for the global myocardium increased from 0.145 in the fasted state to 0.459  $\mu\text{mole}/\text{min}/\text{g}$  after glucose as demonstrated by the parametric images. The MMRGlc was relatively well preserved in the hypoperfused myocardial regions in the anterior wall (0.127 to 0.297  $\mu\text{mole}/\text{min}/\text{g}$ ) and is increased in the

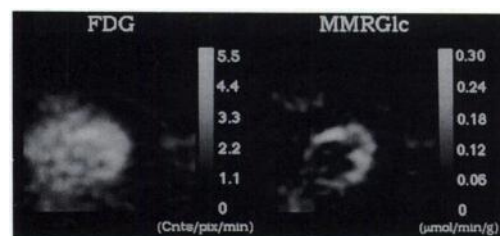


**FIGURE 5.** Comparison of an FDG uptake image (left) to a MMRGlc parametric image (right) in a patient with low myocardial glucose uptake. Myocardium is clearly defined in parametric image, but only poorly on the FDG uptake image.

**TABLE 2**  
Comparison of MMRGlc Values

Patient	Parametric Imaging	Regional Analysis	
		Nonlinear	Patlak
1	0.636 ± 0.070*	0.636 ± 0.089†	0.688 ± 0.004‡
2	0.393 ± 0.030	0.389 ± 0.038	0.399 ± 0.011
3	0.453 ± 0.045	0.458 ± 0.060	0.414 ± 0.010
4	0.510 ± 0.112	0.445 ± 0.076	0.472 ± 0.009
5	0.499 ± 0.061	0.431 ± 0.053	0.536 ± 0.025
6	0.463 ± 0.074	0.461 ± 0.020	0.510 ± 0.014
7	0.795 ± 0.238	0.760 ± 0.066	0.725 ± 0.016
8	0.472 ± 0.052	0.406 ± 0.051	0.439 ± 0.012
9	0.166 ± 0.019	0.151 ± 0.022	0.165 ± 0.005
10	0.193 ± 0.022	0.212 ± 0.031	0.202 ± 0.015
11	0.344 ± 0.026	0.316 ± 0.033	0.375 ± 0.006
Mean	0.448 ± 0.179‡	0.424 ± 0.171‡	0.448 ± 0.172‡

\* Mean value ± standard deviation of pixel values in a global left ventricular myocardium ROI in units of  $\mu\text{mole}/\text{min}/\text{g}$ .

† Estimated value ± standard error of the estimate in units of  $\mu\text{mole}/\text{min}/\text{g}$ .

‡ Mean value ± standard deviation of MMRGlc of 11 studies in units of  $\mu\text{mole}/\text{min}/\text{g}$ .

Six time points were used in each subject for generating the above results of parametric imaging and regional Patlak analysis approaches.

normal interventricular septum (0.101 to 0.499  $\mu\text{mole}/\text{min}/\text{g}$ ).

MMRGlc values for normal, hypoperfused with preserved metabolism and hypoperfused with reduced glucose utilization myocardial regions were  $0.503 \pm 0.171$ ,  $0.469 \pm 0.158$  and  $0.179 \pm 0.050$   $\mu\text{mole}/\text{min}/\text{g}$  for eight nondiabetic patients studied after oral glucose administration with both  $^{13}\text{NH}_3$  and FDG. These regional MMRGlc values were obtained by ROI analysis of parametric images.

Figure 7 illustrates circumferential profiles of  $^{13}\text{NH}_3$ ,

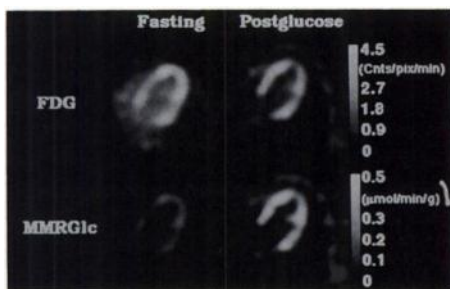


**FIGURE 6.** Fasting and postglucose FDG studies 49 min after FDG injection (upper panels) are displayed on the same scale of counts/pixel/min. The corresponding MMRGlc parametric images are shown in the lower panels using units of  $\mu\text{mol}/\text{min}/\text{g}$ . Globally increased MMRGlc in the postprandial study is demonstrated in MMRGlc parametric images. Relatively preserved MMRGlc in the hypoperfused myocardial regions in the anterior wall and the increased MMRGlc in normal myocardium is well visualized in the parametric images.

FDG and MMRGlc from a single plane in one patient. Also included are profiles of the differences between FDG and  $^{13}\text{NH}_3$  and MMRGlc and  $^{13}\text{NH}_3$ .

## DISCUSSION

While noise in the dynamic study and the computational burden of the nonlinear fitting approach render a pixel-by-pixel nonlinear regression estimation of MMRGlc impractical, Patlak graphical analysis of kinetic FDG image data is highly suitable for generation of MMRGlc parametric images because of its computational simplicity, provided the same lumped constant can be used for normal and pathologic regions.

The shape of the input function was generated from ROIs over the left ventricular blood pool, while a limited number of plasma samples were required for correction of spillover of activity from the myocardial tissue to chamber. Assignment of the ROI to the left ventricular blood pool should be made with caution in order to minimize three-dimensional spillover from tissue to the left ventricular chamber,  $\text{SP}_{\text{TC}}$ , which is most significant at late scan times.

As  $k_4^*$  increases, the relative error produced by violating the assumption inherent to the Patlak analysis requiring the tracer to be irreversibly trapped in myocardium becomes larger. This violation causes bending of the Patlak plot and thus, underestimation of the K value. This underestimation produced by a non-zero  $k_4^*$  can be significant as shown in Figure 2. Therefore,  $k_4^*$  should be estimated before applying this approach in a routine basis.

Global myocardial ROI kinetic data can be used to obtain  $k_4^*$  because very little regional variation in  $k_4^*$  for normal and pathologic tissue was evident in our data. With the 54 min FDG acquisition sequence used in this work, the effect of  $k_4^*$  on the results ranged from a minimum of no effect in most slices ( $k_4^*$  not significantly different from zero) to a maximum of 9% in one case. In longer acquisition sequences, the effect of  $k_4^*$  would be expected to be more significant.

If the  $k_4^*$  value is known in advance to be small ( $<0.002$   $\text{min}^{-1}$  which causes about 5% difference in MMRGlc), the nonlinear regression procedure is not needed. In this case, the value of  $\text{SP}_{\text{CT}}$  can be approximated to be 0.17 (a nominal value obtained in this study). The effect of any error in  $\text{SP}_{\text{CT}}$  on estimated  $C_p^*(t)$  and on MMRGlc is very small, because  $\text{SP}_{\text{CT}}$  is only dominant early after tracer injection which corresponds to image frames not used for calculating the Patlak plot, and also because  $\text{SP}_{\text{CT}}$  affects only the y intercept but not the slope of the Patlak plot (11).

The choice of the number of image sets (tissue data points) used for the analysis depends on the relative emphasis attached to computational time, quantitative accuracy and noise in the generated parametric images. Accurate and reproducible values of MMRGlc and good image quality of parametric images were obtained with a few as

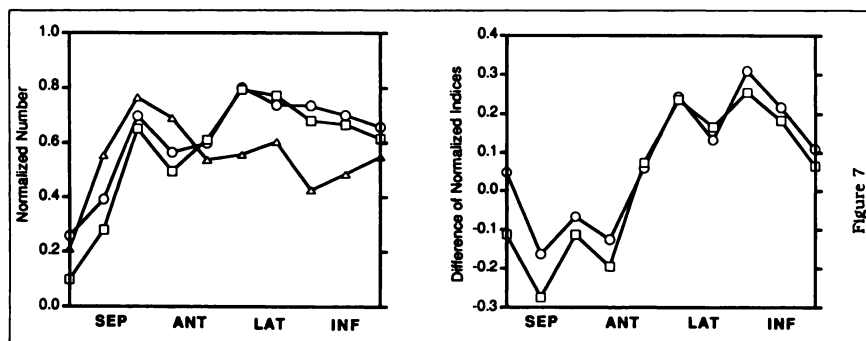


**FIGURE 7.** (Left) Activity profiles of  $^{13}\text{NH}_3$  (triangles) and FDG (circles), and MMRGlc (squares) for the cross-sectional images. (Right) Comparison of FDG- $^{13}\text{NH}_3$  (circles) and MMRGlc- $^{13}\text{NH}_3$  (squares) indices. Ten circumferential segmental values of septal (SEP), lateral (LAT), anterior (ANT), and inferior (INF) wall from the images of  $^{13}\text{NH}_3$ , FDG, and MMRGlc were normalized to maximum pixel value of their respective images.

three scan time points in good quality FDG studies. The standard error of MMRGlc for 22, 11, 6, and 3 image sets was within 6%.

On Figure 7, note the values taken from MMRGlc images are consistently lower than those from FDG images because of spillover of activity correction (left panel) and the wider range of values in the difference profiles for MMRGlc and  $^{13}\text{NH}_3$  as compared to FDG and  $^{13}\text{NH}_3$  (right panel) due to the contrast amplification effect of the parametric imaging method. Because of this effect, quantitative comparison studies with  $^{13}\text{NH}_3$  studies may be possible even in the case of the low MMRGlc.

## CONCLUSIONS

MMRGlc parametric images are computationally practical to generate and improve the image contrast of myocardial FDG studies. This technique has the advantage of facilitating numerical evaluation of myocardial metabolism and compressing numerous image frames of dynamic PET studies, blood sample data, plasma glucose concentration measurements and other parameters required to estimate MMRGlc into a single parametric image. MMRGlc parametric images will be clinically useful, particularly in conditions where estimates of the severity and geometric extent of metabolic abnormalities are important to define.

## ACKNOWLEDGMENTS

This work was supported in part by a Student Fellowship from the Education and Research Foundation of the Society of Nuclear Medicine, DOE contract (#DE-FCO3-87ER60615), and NIH grants (HL 33177 and HL 29845). Dr. Brunken is the recipient of a Clinical Investigator Award (HL 2202-2) from the National Institutes of Health, Bethesda, Maryland. The authors thank Craig Morioka for implementing and testing the speed of the algorithm in a Connection Machine computer.

## REFERENCES

- Sokoloff L, Reivich M, Kennedy C, et al. The [ $^{14}\text{C}$ ]deoxyglucose method for the measurement of local cerebral glucose utilization: theory, procedure, and normal values in the conscious and anesthetized albino rat. *J Neurochem* 1977;28:897-916.
- Gallagher BM, Ansari A, Atkins H, et al. Radiopharmaceuticals XXVII.  $^{18}\text{F}$ -labeled 2-deoxy-2-fluoro-D-glucose as a radiopharmaceutical for measuring regional myocardial glucose metabolism in vivo: tissue distribution and imaging studies in animals. *J Nucl Med* 1977;18:990-996.
- Hawkins RA, Phelps ME, Huang SC. Effects of temporal sampling, glucose metabolic rates and disruptions of the blood-brain barrier on the FDG model with and without a vascular compartment: studies in human brain tumors with PET. *J Cereb Blood Flow Metab* 1986;6:170-183.
- Huang SC, Phelps ME, Hoffman EJ, et al. Noninvasive determination of local cerebral metabolic rate of glucose in man. *Am J Physiol* 1980;238:E69-E82.
- Phelps ME, Hoffman EJ, Selin CE, et al. Investigation of [ $^{18}\text{F}$ ]2-fluoro-2-deoxyglucose for the measurement of myocardial glucose metabolism. *J Nucl Med* 1978;19:1311-1319.
- Schwaiger M, Huang SC, Krivokapich J, et al. Myocardial glucose utilization measured noninvasively in man by positron tomography [Abstract]. *J Am Coll Cardiol* 1983;1:688.
- Krivokapich J, Huang SC, Phelps ME, et al. Estimation of rabbit myocardial metabolic rate for glucose using fluorodeoxyglucose. *Am J Physiol* 1982;243:H884-H895.
- Krivokapich J, Huang SC, Selin CE, et al. Fluorodeoxyglucose rate constants, lumped constant, and glucose metabolic rate in rabbit heart. *Am J Physiol* 1987;252:H777-H787.
- Ratib O, Phelps ME, Huang SC, et al. Positron tomography with deoxyglucose for estimating local myocardial glucose metabolism. *J Nucl Med* 1982;23:577-586.
- Choi Y, Hawkins RA, Huang SC, et al. Parametric images of myocardial glucose utilization generated from dynamic cardiac FDG-PET studies [Abstract]. *J Nucl Med* 1989;30:735.
- Gambhir SS, Schwaiger M, Huang SC, et al. Simple noninvasive quantification method for measuring myocardial glucose utilization in humans employing positron emission tomography and fluorine-18-deoxyglucose. *J Nucl Med* 1989;30:359-366.
- Weinberg IN, Huang SC, Hoffman EJ, et al. Validation of PET-acquired input functions for cardiac studies. *J Nucl Med* 1988;29:241-247.
- Phelps ME, Huang SC, Hoffman EJ, et al. Tomographic measurement of local cerebral glucose metabolic rate in humans with [ $^{18}\text{F}$ ]2-fluoro-2-deoxy-D-glucose: validation of method. *Ann Neurol* 1979;6:371-388.
- Patlak CS, Blasberg RG, Fenstermacher JD. Graphical evaluation of blood-to-brain transfer constants from multifunctional-time uptake data. *J Cereb Blood Flow Metab* 1983;3:1-7.
- Patlak CS, Blasberg RG. Graphical evaluation of blood-to-brain transfer constants from multifunctional-time uptake data. Generalizations. *J Cereb Blood Flow Metab* 1985;5:584-590.
- Hillis WD. The connection machine. *Scientific American* 1987;256:108-115.